



HAL
open science

Measurement of solute diffusivities. Part I. Analysis of coupled solute buoyancy-driven convection and mass transport

Duncan Maclean, Thierry Alboussiere

► **To cite this version:**

Duncan Maclean, Thierry Alboussiere. Measurement of solute diffusivities. Part I. Analysis of coupled solute buoyancy-driven convection and mass transport. *International Journal of Heat and Mass Transfer*, 2001, 44 (9), pp.1639-1648. 10.1016/S0017-9310(00)00308-2. hal-00203591

HAL Id: hal-00203591

<https://hal.science/hal-00203591>

Submitted on 10 Jan 2008

HAL is a multi-disciplinary open access archive for the deposit and dissemination of scientific research documents, whether they are published or not. The documents may come from teaching and research institutions in France or abroad, or from public or private research centers.

L'archive ouverte pluridisciplinaire **HAL**, est destinée au dépôt et à la diffusion de documents scientifiques de niveau recherche, publiés ou non, émanant des établissements d'enseignement et de recherche français ou étrangers, des laboratoires publics ou privés.

Measurement of solute diffusivities. Part I. Analysis of coupled solute buoyancy-driven convection and mass transport.

D. J. Maclean and T. Alboussière.
Department of Engineering, University of Cambridge,
Cambridge, CB2 1PZ, UK.

July 16, 1999

Abstract

An effective diffusivity model is developed for mass transport by molecular diffusion and unsteady solute buoyancy-driven convection in a horizontal capillary by a method similar to that used for Taylor dispersion in forced flow. A 1D non-linear diffusion equation is obtained and an analytical asymptotic solution is found for dominant convective mass transport, the solution for dominant molecular diffusion is already well known. Both the effective diffusivity model and the asymptotic solutions are validated numerically. A scaling analysis clarifies the boundary between dominant molecular diffusion and dominant convective mass transport. The use of a steady vertical magnetic field for liquid metals and semi-conductors is found to damp the convective mass transport by a factor of Ha^{-4} where Ha is the Hartmann number, characterising the MHD problem.

Nomenclature

B	imposed magnetic field
c	dimensionless alloy composition
C	alloy composition
C_r	reference composition
D	coefficient of molecular diffusion
D_e	coefficient of effective diffusivity
g	gravity
H, L	height and length of cavity
j	dimensionless electric current density
p	dimensionless pressure
t	dimensionless time
T	time
v	dimensionless velocity vector
V	velocity vector
v_x	dimensionless axial component of velocity
V_x, V_y	axial and lateral components of velocity
x, y	dimensionless horizontal and vertical coordinates
X, Y	horizontal and vertical coordinates

Greek symbols

α	function of Ha , defined in the text
β	solubility expansion coefficient
δ	dimensionless diffusion length
ΔC	initial step concentration in dopant
Γ	diffusion length
ν	kinematic viscosity
ϕ	dimensionless electric potential
ρ	density
σ	electrical conductivity

Dimensionless groups

A	$Gr_s Sc / Ha^2$
Gr_s	solubility Grashof number ($\beta \Delta C g H^3 / \nu^2$)
Ha	Hartmann number ($BH \sqrt{\sigma / \rho \nu}$)
Sc	Schmidt number (ν / D)

Superscripts

* denotes alternative dimensionless scaling

1 Introduction

The accurate measurement of molecular diffusivities is important for various applications [1], it is however often difficult to achieve in practice as diffusive mass fluxes are generally so low that even very small levels of convection can significantly affect experimental results. One possible solution is to quantify and hence account for the convective mass transport.

Taylor devised a method of achieving this [2] for a fluid moving slowly under forced convection through a capillary to which a solvent is introduced at some position in the flow causing an initial one-dimensional step-difference in composition. He investigated the subsequent dispersion of the solvent arising from the combined effects of molecular diffusion and the lateral variation in the Poiseuille velocity field. It was then possible, subject to certain conditions¹, to describe the lateral average concentration of the solvent by a one-dimensional pure diffusion equation in time and a spatial-axis which moves with the mean velocity of the flow. The virtual coefficient of diffusion, as he called it, is $\frac{1}{4}H^2u^2/(192D)$, where H, u and D are the diameter of the capillary, mean flow velocity and molecular diffusivity respectively.

Taylor's analysis for simple Poiseuille flow is very similar to that of the so called *effective diffusivity model* which was first proposed by Garandet *et al.* [3] in order to account for thermal buoyancy-driven convection and applied by them to the shear-cell technique which is shown schematically in figure 1. They found that for a steady and axially uniform velocity field driven by a lateral temperature gradient in a vertical capillary subject to an initial axial concentration step, the problem could again be reduced to a one-dimensional diffusion equation in lateral average concentration. The effective diffusivity is $D(1+\epsilon(Hu/D)^2)$ where u is now the mean absolute velocity (convection being parallel counter-flow) and ϵ is some constant which they estimated by orders of magnitude as 1/4 for a 2D capillary. Similar results are found by Alboussi re *et al.* [4] for a horizontal cavity subject to an axial temperature gradient, they also consider an electrically conducting liquid and a steady vertical magnetic field to damp convection. In each case the additional convective contribution to mass transport scales with H^2u^2/D and the constant ϵ , of order unity, depends on the general form of the velocity profile assumed (e.g. cubic Birikh, linear high Hartmann etc).

In practice however, density differences arising from variations in composition are likely to have a significant contributory effect on convection. Barat & Garandet [5] considered a vertical capillary with a lateral temperature gradient and an initial step concentration with a heavier liquid on the bottom so that solute buoyancy forces tend to damp thermally driven convection. They found through scaling analysis and numerical simulations that even when composition density

¹The conditions were effectively that the axial mass transport is predominantly convective and the typical convective timescale is large compared to the time for diffusion to extend over one diameter of the capillary.

differences were quite small, there is a noticeable time-dependant damping effect on convection and for larger composition density differences the velocity field is no longer axially uniform. The general form of the expression for effective diffusivity remains unchanged where there is solutal buoyancy-driven convection, but the average-velocity term within the expression becomes a function of time and axial space because it depends on the unsteady and non-uniform concentration gradient. The resulting one-dimensional diffusion equation in lateral average concentration is therefore no longer linear.

The case of solute buoyancy-driven convection along with molecular diffusion in a horizontal isothermal long capillary subject to an axial composition-step is considered in this paper. The liquid is electrically conducting and the capillary is placed in a vertical magnetic field, though the asymptotic case of the Hartmann number going to zero is accounted for so the results equally apply to there being no magnetic field. An idealised two-dimensional configuration is described in section 2 and the corresponding non-linear one-dimensional effective diffusivity model is developed in section 3. Separate asymptotic solutions corresponding to convective mass transport dominating molecular diffusion and vice-versa are then derived in section 4 and these are validated numerically using CFX, a commercial CFD code in section 5. An orders of magnitude analysis is used in section 6 to justify some assumptions made in the earlier analysis and finally a discussion of the results and the work required to extend the model to a three dimensional capillary are presented in section 7.

2 Configuration

A horizontal two dimensional cavity of length L and height H is considered with $L \gg H$. This capillary contains a carrier fluid and a dopant of composition $C = C_r$ with an initial step concentration of ΔC at its central cross-section. Convection is driven by the density differences arising from variations in composition. The capillary is placed in a steady vertical magnetic field of strength \mathbf{B} . A schematic of the set-up with typical velocity and concentration profiles are shown in figure 2.

The coefficient of molecular diffusion D , and the fluid properties kinematic viscosity ν , coefficient of solutal expansion β and electrical conductivity σ are all assumed independent of composition. Density, ρ , and the governing equations are subject to the Boussinesq approximation.

Using the scales H , D/H , $\rho D^2/H^2$, H^2/D , $B\sigma D/H$, BD and ΔC for length x , velocity \mathbf{v} , pressure p , time t , electric current density \mathbf{j} , electric potential ϕ and concentration c , and assuming that the magnetic Reynolds number is small, the dimensionless Navier-Stokes, continuity, mass transport, Ohm's law and electric

charge conservation equations are:

$$\frac{1}{Sc} \left(\frac{\partial \mathbf{v}}{\partial t} + (\mathbf{v} \cdot \nabla) \mathbf{v} \right) = -\frac{1}{Sc} \nabla p + Ha^2 \mathbf{j} \times \frac{\mathbf{B}}{B} + \nabla^2 \mathbf{v} + Gr_s Sc \frac{\mathbf{g}}{g} c, \quad (1)$$

$$\nabla \cdot \mathbf{v} = 0, \quad (2)$$

$$\frac{\partial c}{\partial t} + (\mathbf{v} \cdot \nabla) c = \nabla^2 c, \quad (3)$$

$$\mathbf{j} = -\nabla \phi + \mathbf{v} \times \frac{\mathbf{B}}{B}, \quad (4)$$

$$\nabla \cdot \mathbf{j} = 0. \quad (5)$$

The non-dimensional groups appearing in these equations are: Hartmann number $Ha = BH \sqrt{\sigma / \rho \nu}$, Schmidt number $Sc = \nu / D$ and solutal Grashof number $Gr_s = \beta \Delta C g H^3 / \nu^2$.

The boundary conditions at the walls arising from no-slip, zero mass transport across walls and electrically insulating walls become:

$$\mathbf{v} = 0, \quad \frac{\partial c}{\partial \eta} = 0, \quad \frac{\partial \phi}{\partial \eta} = 0,$$

where η is the normal direction to the walls. The initial conditions are, at $t = 0$:

$$\mathbf{v} = 0; \quad c(x < 0) = 0; \quad c(x > 0) = 1.$$

It was shown by Garandet *et al.* [6] that for such a 2D cavity, the electric potential is uniform ($\nabla \phi = 0$) and so the Lorentz force reduces to a damping factor $-B^2 v_x \mathbf{x}$ where $v_x \mathbf{x}$ is the axial component of \mathbf{v} .

3 Effective Diffusivity

The objective here is to reduce the coupled two dimensional governing equations (1) to (5) into a single one dimensional diffusion equation in lateral average concentration as a function of axial position and time. The concentration field, $c(x, y, t)$ is broken down into components $c_0(x, t)$ representing the average of c over a lateral cross-section of the capillary and $c_1(x, y, t)$ representing the perturbation from the average. This can be expressed as $c_0 = \langle c \rangle_s$ and $c_1 = c - c_0$ where $\langle \rangle_s$ denotes average over a lateral cross-section.

Averaging equation (3) in a similar manner and making use of the boundary conditions for velocity and concentration yields:

$$\frac{\partial c_0}{\partial t} + \frac{\partial \langle v_x c_1 \rangle_s}{\partial x} = \frac{\partial^2 c_0}{\partial x^2}, \quad (6)$$

It is now required to find expressions for c_1 and v_x as a functions of c_0 which can be substituted into equation (6) to give an equation only in c_0 . Subtracting equation (6) from equation (3) gives:

$$\frac{\partial c_1}{\partial t} + \mathbf{v} \cdot \nabla c_0 + \mathbf{v} \cdot \nabla c_1 - \frac{\partial \langle v_x c_1 \rangle_s}{\partial x} - \nabla^2 c_1 = 0. \quad (7)$$

It will be shown by order of magnitudes analysis in section 6 that when $t \gg 1$, equation (7) reduces to the following leading terms²:

$$v_x \frac{\partial c_0}{\partial x} = \nabla_s^2 c_1, \quad (8)$$

where $\nabla_s^2 = \frac{\partial^2}{\partial y^2}$. The analysis leading to equation (8) is of the same nature as Taylor's approach [2].

The velocity field is obtained through analogy to work done by Garandet *et al.* [6] on a similar set-up, but where convection was driven by a uniform steady thermal gradient rather than the unsteady non-uniform composition gradient here. Following their method of analysis, using a local concentration gradient $\frac{\partial c_0}{\partial x}$, one finds:

$$v_x = A \frac{\partial c_0}{\partial x} \left(\frac{\sinh(Hay)}{2 \sinh(Ha/2)} - y \right), \quad (9)$$

where $A = \frac{Gr_s Sc}{Ha^2}$. The validity of equation (9) is based on the assumption that $\frac{\partial c}{\partial x}$ is "locally" uniform, i.e. uniform over a cross-section and axially uniform over a distance longer than H . This will be discussed in section 6.

Substituting for v_x into equation (8), integrating twice with respect to y and using $\langle c_1 \rangle_s = 0$ along with the boundary condition $\frac{\partial c_1}{\partial y} = 0$ at $y = \pm \frac{1}{2}$ gives an expression for c_1 depending on $\frac{\partial c_0}{\partial x}$:

$$c_1 = A \left(\frac{\partial c_0}{\partial x} \right)^2 \left(-\frac{y^3}{6} + \frac{Ha \tanh(Ha/2) - 4}{8Ha \tanh(Ha/2)} y + \frac{\sinh(Hay)}{2Ha^2 \sinh(Ha/2)} \right), \quad (10)$$

The convective term in equation (6) can now be calculated from equations (9) and (10):

$$\langle v_x c_1 \rangle_s = -A^2 \left(\frac{\partial c_0}{\partial x} \right)^3 \alpha(Ha), \quad (11)$$

where, denoting $Th = \tanh(Ha/2)$ and $Sh = \sinh(Ha/2)$,

$$\alpha(Ha) = \frac{1}{120} - \frac{1}{12HaTh} + \frac{1}{Ha^2} \left(\frac{1}{4Th^2} + \frac{1}{8Sh^2} \right) + \frac{1}{4Ha^3Th} - \frac{2}{Ha^4}. \quad (12)$$

²This proof is given in section 6 which may be read prior to the remainder of the current section without loss of continuity in the text to the reader.

It is found that as $Ha \rightarrow \infty$, $\alpha A^2 \rightarrow \frac{(Gr_s Sc)^2}{120 Ha^4}$ and as $Ha \rightarrow 0$, $\alpha A^2 \rightarrow \frac{(Gr_s Sc)^2}{326880}$, this can be seen from the plot of $\alpha(Ha)$ against Ha in figure 3. These limits respectively agree with the solutions obtained for equation (11) if the linear high Hartmann velocity of Garandet *et al.* [6] or the cubic velocity in the absence of a magnetic field of Birikh [7] are used in place of v_x from equation (9).

Substituting for $\langle v_x c_1 \rangle_s$, equation (6) becomes after rearrangement:

$$\frac{\partial c_0}{\partial t} = \frac{\partial}{\partial x} \left\{ \left[1 + \alpha A^2 \left(\frac{\partial c_0}{\partial x} \right)^2 \right] \frac{\partial c_0}{\partial x} \right\}. \quad (13)$$

This expression represents a one dimensional diffusion equation in c_0 valid for $t \gg 1$. The dimensionless coefficient of *effective diffusivity* is $D_e(x, t)/D = \left[1 + \alpha A^2 \left(\frac{\partial c_0}{\partial x} \right)^2 \right]$. The equation is characterised by the dimensionless parameters of the system encompassed within the term αA^2 . By rescaling the length and time with $t^* = \frac{1}{\alpha A^2} t$ and $x^* = \frac{1}{\sqrt{\alpha A^2}} x$ respectively, a universal equation valid for $t^* \gg \frac{1}{\alpha A^2}$ but which is otherwise independent of all system parameters is obtained:

$$\frac{\partial c_0}{\partial t^*} = \frac{\partial}{\partial x^*} \left\{ \left[1 + \left(\frac{\partial c_0}{\partial x^*} \right)^2 \right] \frac{\partial c_0}{\partial x^*} \right\}. \quad (14)$$

4 Asymptotic solutions

In equation (14), the term $\left(\frac{\partial c_0}{\partial x^*} \right)^2$ represents the convective contribution to effective diffusivity, it is the mass transport over and above the pure molecular diffusion which would otherwise occur in the absence of convection. Contrary to the case of thermal buoyancy-driven convection where the convective contribution to effective diffusivity is steady and constant, it is here a function of both space and time. At small t^* , this term is large (and indeed tends to infinity at $x^* = 0$ as $t^* \rightarrow 0^+$) and the convective contribution will dominate molecular diffusion. In the middle of the cavity, the term monotonically decreases with time and will eventually be small compared to unity, after which molecular diffusion will dominate the convective contribution. By orders of magnitude on equation (14), considering both $\left(\frac{\partial c_0}{\partial x^*} \right)^2 \gg 1$ and $\left(\frac{\partial c_0}{\partial x^*} \right)^2 \ll 1$ it is found that the transition between the two regimes must occur at $t^* \sim 1$. Equation (14) is however only valid for $t^* \gg \frac{1}{\alpha A^2}$ so the transition between the two asymptotic regimes could, depending on the parameters of the system, occur before or after this time. Solutions are now derived for the two asymptotic regimes.

Considering first the case where $\left(\frac{\partial c_0}{\partial x^*} \right)^2 \ll 1$, equation (14) reduces to:

$$\frac{\partial c_0}{\partial t^*} = \frac{\partial^2 c_0}{\partial x^{*2}}. \quad (15)$$

The solution to this equation for a step input is well known [8], though more commonly as applied to the analogous case of a semi-infinite solid subject to a step-input constant surface temperature:

$$c_0(x^*, t^*) = \frac{1}{2} [1 + \operatorname{erf}(\kappa)], \quad (16)$$

$$\frac{\partial c_0}{\partial x^*} = \frac{1}{2\sqrt{\pi}} t^{*-1/2} e^{-\kappa^2}, \quad (17)$$

where $\kappa(x^*, t^*) = \frac{x^*}{2\sqrt{t^*}}$.

The second case, when t^* is “small” and so $\left(\frac{\partial c_0}{\partial x^*}\right)^2 \gg 1$ leads to the following non-linear form for equation (14):

$$\frac{\partial c_0}{\partial t^*} = \frac{\partial}{\partial x^*} \left[\left(\frac{\partial c_0}{\partial x^*} \right)^3 \right]. \quad (18)$$

Substituting $f(x^*, t^*) = \frac{\partial c_0}{\partial x^*}$ and differentiating (18) with respect to x^* :

$$\frac{\partial f}{\partial t^*} = \frac{\partial^2 f^3}{\partial x^{*2}}. \quad (19)$$

A self-similar solution is now sought of the form $f(x^*, t^*) = g(t^*)h(\eta)$ where $\eta = g(t^*)x^*$ and $\int_{-\infty}^{+\infty} h d\eta = 1$ since c_0 varies from 0 to 1 when x varies from $-\infty$ to $+\infty$. Substituting for f into (19), dividing by $g^5 h$ and rearranging gives:

$$\frac{g'}{g^5} = \frac{3hh'' + 6h'^2}{\left[1 + \eta \frac{h'}{h}\right]}, \quad (20)$$

the right hand side of this expression a function of $\eta(x^*, t^*)$, the left hand side however is only a function of t^* and both sides of the equation must therefore be constant, so

$$g = K t^{*-1/4}. \quad (21)$$

Any choice for the constant K would be valid and accommodated for in h , $K = 1$ is chosen here. Substituting $f = t^{-1/4}h$, equation (20) after some manipulation becomes:

$$-\frac{1}{4} [\eta h]' = [h^3]'' . \quad (22)$$

Integrating this once with respect to η and choosing a zero constant of integration so that h is an even function ($h'(0) = 0$) since the spatial concentration gradient must be a maximum at $x^* = 0$:

$$-\frac{1}{4} \eta h = 3h^2 h'. \quad (23)$$

Ignoring the trivial solution $h = 0$ and dividing by h then integrating with respect to η gives:

$$\frac{1}{12}\eta^2 + h^2 = C^2, \quad (24)$$

where C is a constant. This is the equation for an ellipse, centred at the origin, the constant C is obtained from the requirement that $\int_{-\infty}^{+\infty} h d\eta = 1$, implying that the area under the half-ellipse is 1 which gives $C^2 = \frac{1}{\sqrt{3}\pi}$. The solution for h , which is valid until $h = 0$ since its derivation required division by h , is then:

$$h(\eta) = \sqrt{\frac{1}{\sqrt{3}\pi} + \frac{\eta^2}{12}}. \quad (25)$$

This is one possible solution for $h(\eta)$, satisfying equation (22) on the interval $[-2(\sqrt{3}/\pi)^{1/2}, +2(\sqrt{3}/\pi)^{1/2}]$ which represents the extent of transport of the dopant, outside this interval the function can be continued with $h(\eta) = 0$ without loss of continuity for h . The function h is by definition $\frac{\partial c_0}{\partial \eta}$, the solution for the spatial derivative of c_0 in this asymptotic regime though now becomes:

$$\frac{\partial c_0}{\partial x^*} = t^{*-1/4} \sqrt{\frac{1}{\sqrt{3}\pi} + \frac{\eta^2}{12}}, \quad (26)$$

and c_0 is obtained by integrating h with respect to η with the condition $c_0 = 1/2$ at $\eta = 0$ (i.e. at $x^* = 0$):

$$c_0 = \frac{1}{2} + \frac{\eta}{2} \sqrt{\frac{1}{\sqrt{3}\pi} + \frac{\eta^2}{12}} - \frac{1}{\pi} \arcsin\left(\frac{\sqrt{\pi}\eta}{2\sqrt{3}}\right). \quad (27)$$

Figure 4 shows a graphical representation of h and c_0 against η . The concentration profile looks similar to the error function solution of the pure diffusion case (equation (16)) though now of finite extent $|\eta| \leq 2\sqrt{\sqrt{3}/\pi}$. The role of $e^{-\kappa^2}$ in equation (17) is played here by h with its semi-ellipse replacing the classic ‘bell’ curve of pure diffusion. The maximum of $\frac{\partial c_0}{\partial x^*}$ is always in the middle of the cavity, it now decreases as $t^{-1/4}$ as oppose to $t^{-1/2}$ for pure diffusion.

5 Numerical Simulations

Numerical solutions were obtained independently, for the universal one dimensional equation in c_0 (14), and for the full set of governing equations (1) to (5) using the commercial CFD code, CFX. Checks were made that the final solutions did not depend on spatial or time discretization and that the dopant had not reached the ends of the cavity.

Equation (14) was solved as a molecular-diffusion problem but with the coefficient of diffusion being dynamically modified on each iteration to account for

the additional effective diffusivity as a function of local concentration gradient. The grid ran from $x^* = -50$ to $+50$, discretized into 600 cells with geometric progressions being used to concentrate the mesh around the position of the initial step-concentration at $x^* = 0$.

The full set of governing equations (1) to (5) were solved in their dimensionless form in a cavity of aspect ratio $L/H = 100$ with an initial unit step-concentration at the centre. Typical grids were 500×50 with geometric progressions to concentrate the grid close to the step-concentration and where necessary close to the horizontal walls to catch the Hartmann layers. The parameters specified for each run were Gr_s, Sc and Ha , each of which could be independently varied. Results are presented here from two different configurations: $Gr_s = 1420, Sc = 167, Ha = 15.8$ corresponding to $\alpha(Ha)A^2 = 3669$ and $Gr_s = 4, Sc = 100, Ha = 15.8$ corresponding to $\alpha(Ha)A^2 = 0.01$.

A dimensionless length scale, $\delta(t) = 1/\frac{\partial c_0}{\partial x}|_{x=0}$, which is a measure of the axial distance over which the dopant has spread is defined as shown schematically in figure 5. This is then used as one means of comparing the results between the analytical and numerical models for diffusion. Figure 6 summarises results for development of diffusion length with time from the two asymptotic models, the numerical simulation of the 1D universal equation and the two particular 2D numerical runs. The graph is in terms of the universal coordinate system, (x^*, t^*) defined in section 4 with $\delta^* = \frac{1}{\sqrt{\alpha A}}\delta$.

The effective diffusivity model applied to the 2D problem is valid when $t^* \gg 1/(\alpha A^2)$ as shown in the next section. The numerical results presented here give examples of this occurring before and after the transition from effective diffusivity to molecular diffusion with $\alpha A^2 = 3669$ and $\alpha A^2 = 0.01$ respectively. At $\alpha A^2 = 3669$, the numerical results show good agreement with the asymptotic solution for effective diffusivity shortly after $t^* = 1/(\alpha A^2)$. As expected, the solution then follows the 1D numerics as this departs from the asymptotic model. The run was stopped when diffusion had extended the length of the cavity.

Inspection of equations (17) and (26) shows that the two asymptotic solutions for δ^* intersect at $t^* = \frac{3}{16}$, the 1D numerical solution agrees well with the asymptotic models from about one decade in time either side of this interception point.

The second 2D model, with $\alpha A^2 = 0.01$, shows good agreement with the asymptotic solution for pure diffusion a long time before the validity of the effective diffusion model. This is because for small (enough) values of αA^2 convective mass transport will be dominated by molecular diffusion and the global diffusive solution is obtained irrespective of whether or not the convective contribution follows the effective diffusivity model.

It can be seen from figure 7 that in the effective diffusivity regime, the numerical solutions for concentration gradient as a function of axial distance show reasonable agreement with the asymptotic model. The difference around $\eta = 0$ for the 2D numerics may be attributed to there being some detectable molecular

diffusion, the reason for this being that the onset of the validity of the effective diffusivity model occurs very close to the beginning of the transition from the effective to pure diffusion regimes. This effect could presumably have been avoided by modelling with a higher value of αA^2 . Both 1D and 2D numerical solutions deviate from the asymptotic model as $h(\eta) \rightarrow 0$. This is expected and is because locally the assumption that $\left(\frac{\partial c_0}{\partial x^*}\right)^2 \gg 1$ in equation (18) becomes false as h and hence $\frac{\partial c_0}{\partial x^*}$ approaches 0, molecular diffusion then has a noticeable effect in smoothing the concentration gradient. The axial velocity profiles in figure 8 were calculated analytically using equations (9) and (26). The agreement with the 2D numerical model is good at $x = 0$, the small difference in maximum velocity may again be attributed to there being some noticeable effects of molecular diffusion for the chosen value of αA^2 . The agreement is reasonable at $x = 12$ which corresponds approximately to the distance diffusion has spread ($\delta = 24$). Close inspection shows however that there is no longer symmetry of the absolute magnitude of velocity about $y = 0$. This is not due to numerical errors, it is because the assumption that $\frac{\partial c_1}{\partial x} \ll \frac{\partial c_0}{\partial x}$ does not hold strictly and $\frac{\partial c_1}{\partial x}$ is not an even function of y when $x \neq 0$.

6 Order of magnitude analysis

The main objective of this section is to show that equation (8) and hence the effective diffusivity model become valid once $t \gg 1$. It is more instructive to work in dimensional terms here, whereby the equivalent criteria is that dimensional time, $T \gg H^2/D$.

For all time, denoting the dimensional diffusion length as $\Gamma(T) = \delta H$ where δ is the corresponding dimensionless diffusion length defined in figure 5, the dimensional axial velocity, V_x can be estimated from Garandet *et al.* [6] as:

$$V_x \sim \alpha^{1/2} A \frac{D}{\Gamma}. \quad (28)$$

Where $\alpha^{1/2} A \sim Gr_s Sc$ for $Ha = 0$ and $\alpha^{1/2} A \sim Gr_s Sc / Ha^2$ for $Ha \gg 1$, the parameters α and A are defined more rigorously in section 3. The magnitudes of diffusion length and velocity are first considered for $T \ll H^2/D$. It is possible during this phase, depending on the parameters of the system, that mass transport will be dominated by either diffusion or by convection. In the case of convective mass transport being dominant, the concentration discontinuity will be a thin line distorted by the velocity field and the growth of Γ with time is:

$$\frac{\partial \Gamma}{\partial T} \sim V_x \quad (29)$$

Solving equations (28) and (29) and integrating Γ over time gives approximations

for V_x and Γ during this initial convective phase:

$$\Gamma \sim \sqrt{2\alpha^{1/2}ADT}, \quad (30)$$

$$V_x \sim \sqrt{\frac{\alpha^{1/2}AD}{2T}}. \quad (31)$$

It can be seen from the numerical results in figure 6 that for $\alpha A^2 \gg 1$ and $T \ll H^2/D$ (corresponding to $t^* \ll \frac{1}{\alpha A^2}$ in the figure), the slope of the logarithmic plot of diffusion length against time is approximately $\frac{1}{2}$ in agreement with equation (30). If however molecular diffusion dominates convection during the initial phase, then both during and after this phase,

$$\Gamma \sim \sqrt{DT} \quad (32)$$

and from equation (28),

$$V_x \sim \alpha^{1/2}A\sqrt{\frac{D}{T}}. \quad (33)$$

Comparing equations (30) and (32) shows that convection will dominate during the initial phase if $\sqrt{\alpha^{1/2}A} \gg 1$ and diffusion will dominate if $\sqrt{\alpha^{1/2}A} \ll 1$. Of particular interest and use in the subsequent analysis though is that whichever scenario is dominant, and even if there is a transition from the dominance of convective to diffusive mass transport, be this before or after the initial phase, when $T \gg H^2/D$:

$$\Gamma \gg H, \quad (34)$$

and either dividing equations (31) by (30) or dividing equations (33) by (32), noting that both V_x and $1/\Gamma$ decrease with time,

$$\frac{V_x}{\Gamma} \ll \frac{D}{H^2}. \quad (35)$$

Taking Γ and H as representative length scales for the transport of the dopant in the axial and lateral directions respectively, the validity of the effective diffusivity model can now be shown. The dimensional forms of equations (7) and (8) are:

$$\frac{\partial C_1}{\partial T} + V_x \frac{\partial C_0}{\partial X} + \mathbf{V} \cdot \nabla C_1 - \frac{\partial \langle V_x C_1 \rangle_s}{\partial X} - D \nabla^2 C_1 = 0, \quad (36)$$

$$V_x \frac{\partial C_0}{\partial X} = D \nabla_s^2 C_1. \quad (37)$$

The requirement is that equation (36) reduces to its leading terms in equation (37) when $T \gg H^2/D$. Considering first the order of magnitude of the laplacian of C_1 in equation (36):

$$D \nabla^2 C_1 = D \left[\frac{\partial^2 C_1}{\partial X^2} + \nabla_s^2 C_1 \right] \sim D \left[\frac{C_1}{\Gamma^2} + \frac{C_1}{H^2} \right] \sim D \frac{C_1}{H^2} \quad (38)$$

It can be seen that each of the remaining terms of equation (36) in C_1 are, for $T \gg H^2/D$, much smaller than DC_1/H^2 and can therefore be ignored:

$$\frac{\partial C_1}{\partial T} \sim \frac{C_1}{T} \ll C_1 \frac{D}{H^2}. \quad (39)$$

By continuity $V_y \sim V_x \frac{H}{\Gamma}$, so by equation (35):

$$\mathbf{V} \cdot \nabla C_1, \frac{\partial \langle V_x C_1 \rangle_s}{\partial X} \ll C_1 \frac{D}{H^2}, \quad (40)$$

and hence taking only the remaining dominant terms, equation (36) reduces to equation (37) as required.

The derivation of equation (9) is based on $\frac{\partial c}{\partial x}$ being ‘‘locally’’ uniform, this can now be shown to be true for $T \gg H^2/D$. Equation (37) implies that, $C_1 \sim (V_x C_0 H^2)/(D\Gamma)$, which by equation (35) means that $C_1 \ll C_0$ and so $\frac{\partial C}{\partial X} \approx \frac{\partial C_0}{\partial X}$ and $\frac{\partial C}{\partial X}$ is therefore uniform over a cross section. Axial variations of C occur over a typical length-scale of Γ , and since $\Gamma \gg H$, $\frac{\partial C}{\partial X}$ is also axially uniform over a distance longer than H .

It is interesting to return to the estimates of the diffusion length during the initial stage (for $T \ll H^2/D$) and in particular its continuity through the transition to the effective diffusivity model. The case of $\sqrt{\alpha^{1/2}A} \ll 1$ is trivial as Γ is predicted by equation (32) for all time. When $\sqrt{\alpha^{1/2}A} \gg 1$, the transport length during the initial convective stage is predicted by equation (30), the diffusion length can also be estimated for the effective diffusion phase from equation (26):

$$\Gamma \sim \sqrt{\alpha^{1/2}AH} (DT)^{1/4}. \quad (41)$$

At the time of the transition from convective to effective diffusive mass transport (i.e. $T \sim H^2/D$), both of these approximations become $\Gamma \sim \sqrt{\alpha^{1/2}AH}$. This implies that after a few H^2/D the initial convective phase will be smoothed out by effective diffusion and its influence on diffusion length negligible.

7 Discussion and conclusions

A non-linear one-dimensional effective diffusivity model has been developed to describe the combined effects of molecular diffusion and solute buoyancy-driven convection in a horizontal isothermal capillary subject to an initial axial step-concentration. Analytical asymptotic solutions were found for this model relating to the two extremes of dominant convective mass transport and dominant diffusive mass transport. A numerical solution of the one-dimensional model agreed well with the asymptotic solutions. Numerical simulations were also performed for the full set of two-dimensional governing equations and there was again good agreement between these and the one-dimensional model.

Through scaling analysis it was shown that the effective diffusivity model becomes valid once $T \gg H^2/D$ in agreement with Taylor [2]. It was further shown that the convective contribution to mass transport will be negligible in comparison to diffusion when the dimensionless group $\alpha A^2 \ll 1$. In the converse case of $\alpha A^2 \gg 1$, convective mass transport will dominate diffusion until $t^* \sim 3/16$, after this time solute buoyancy forces will have decayed sufficiently for diffusion to again dominate. All of these findings agree with the numerical results.

This analysis could be useful in experimental work to determine molecular diffusion coefficients. The solutions obtained for the 2D model are valid in 3D though the group αA^2 must be determined for any particular set-up. By analogy to the case of thermal convection in a horizontal capillary [4] this group is $7(Gr_s Sc)^2/11796480$ when there is no magnetic field and $7A^2/384$ in the high Hartmann limit with a vertical magnetic field, assuming in both cases that there is no convective mass transport within a cross-section (i.e. no stratification of concentration). For intermediate Hartmann numbers the general form of the group is still $\alpha(Ha)A^2$ though analytical solutions have not been obtained. Numerical solutions for the function $\alpha(Ha)$ in the 3D cylinder with no cross-sectional mass transport have however been calculated and are presented in figure 3, the method used for these numerics is briefly described here. Assuming no convective mass transport over a cross-section and ignoring inertia, the governing equations for a cross-section of the capillary can, once the effective diffusivity model is valid, be reduced to:

$$\nabla_s^2 v_x = Ha^2 \left(\frac{\partial \phi}{\partial z} + v_x \right) - Gr_s Sc \frac{\partial c_0}{\partial x} y, \quad (42)$$

$$\nabla_s^2 \phi = -\frac{\partial v_x}{\partial z}, \quad (43)$$

$$\nabla_s^2 c_1 = v_x \frac{\partial c_0}{\partial x}, \quad (44)$$

where $\nabla_s^2 = \frac{\partial^2}{\partial y^2} + \frac{\partial^2}{\partial z^2}$. The CFX package was used to solve equations (42) to (44) numerically on a 2D circular domain with the original boundary conditions described in section 2, α was then determined from equation (11) using the calculated values of v_x and c_1 . This process was repeated for a range of values of Gr_s , Ha and Sc . The value of $\frac{\partial c_0}{\partial x}$ does not affect the calculated value of α . Davoust *et al.* [9] find that when there is stratification and hence convective mass transport within a cross-section, the result for a 3D cylinder in the high Hartmann limit changes by about 5% to $5A^2/288$, implying that the assumption of no stratification is reasonable.

In all cases, the convective contribution to mass transport scales with Ha^{-4} and so the use of magnetic fields where the fluid is an electrical conductor could be a useful means of suppressing unwanted convective effects, which was also shown to be the case where convection is thermally driven [4].

The work could be extended to consider the combination of thermal and solutal driven buoyancy. The governing equations are again highly non linear and the solutions are likely to depend on whether the two driving forces complement or oppose each other as suggested by previous experimental results [4]. Further extensions to the work could be to look at other forces driving convection such as Marangoni, vibrations and g-jitters in space.

The analytical work presented here assumes that inertia will be low and does not account for the possibility of shear-flow instabilities when the solute buoyancy driving force is very high. This situation was observed in the initial stages of some numerical runs (though not the ones presented here) when the group αA^2 is very large, causing recirculation of the flow. It may be expected to cause mixing and hence increase the perceived effective diffusivity. In the numerical runs where it was observed, the effects were eventually smoothed out and undetectable by the start of the effective diffusivity regime though the situation was not investigated in any detail.

Acknowledgements — This work was supported by the EPSRC under grant GR/L84193. The authors thank Dr J.P. Garandet from CEN Grenoble for his many useful comments and advice on the work. The authors also thank Professor R. Moreau, Dr P. Lehmann and Mr V. Botton from MADYLAM for their collaboration and useful discussions, and whose experimental paper on the work will appear as part II. Thanks are also given to the technical support staff at AEA Technology PLC for advice and assistance in the use of CFX for the numerical simulations.

References

- [1] T. Iida and R. L. Guthrie. *The physical properties of liquid metals*. Clarendon Press, Oxford, 1993.
- [2] G. Taylor. Dispersion of soluble matter in solvent flowing slowly through a tube. In *Proc. Roy. Soc. London Sect A*, volume 219, pages 186–203, 1953.
- [3] J. P. Garandet, C. Barat, and T. Duffar. The effect of natural convection in mass transport measurements in dilute liquid alloys. *Int. J Heat Mass Transfer*, 38(12):2169–2174, 1995.
- [4] T. Alboussière, J.P. Garandet, P. Lehmann, and R. Moreau. Convective effects in the measurement of diffusivities and thermotransport coefficients. Liquid metal alloys and the use of a magnetic field. *Entropie*. to appear.

- [5] C. Barat and J. P. Garandet. The effect of natural convection in liquid phase mass transport coefficient measurements: the case of thermosolutal convection. *Int. J Heat Mass Transfer*, 39(10):2177–2182, 1996.
- [6] J. P. Garandet, T. Alboussière, and R. Moreau. Buoyancy-driven convection in a rectangular enclosure with a transverse magnetic field. *Int. J Heat Mass Transfer*, 35(4):741–748, 1992.
- [7] R. V. Birikh. Thermocapillary convection in a horizontal layer of liquid. *J. Appl. Mech. Phys*, 3:69–72, 1966.
- [8] J. Crank. *The Mathematics of Diffusion*. Oxford Press, 1970.
- [9] L. Davoust, M. D. Cowley, R. Moreau, and R. Bolcato. Buoyancy-driven convection with a uniform magnetic field. part ii. experimental investigation. *J. Fluid Mech.* to appear.

Captions & Figures

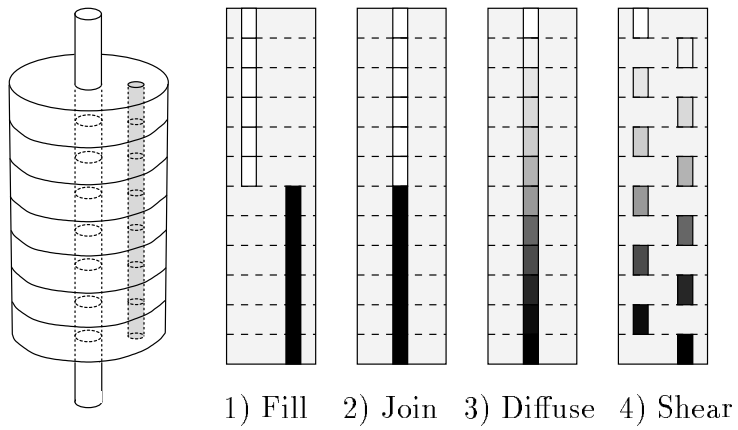


Figure 1: Schematic of the Shear cell technique: 1) Two capillaries are filled with liquids of different compositions. 2) The capillaries are joined giving a step-composition at the interface. 3) Diffusion and/or convective mass transport occurs. 4) The capillary is sheared, each shear-sample is solidified and globally analysed to give a 1D variation of composition with axial distance

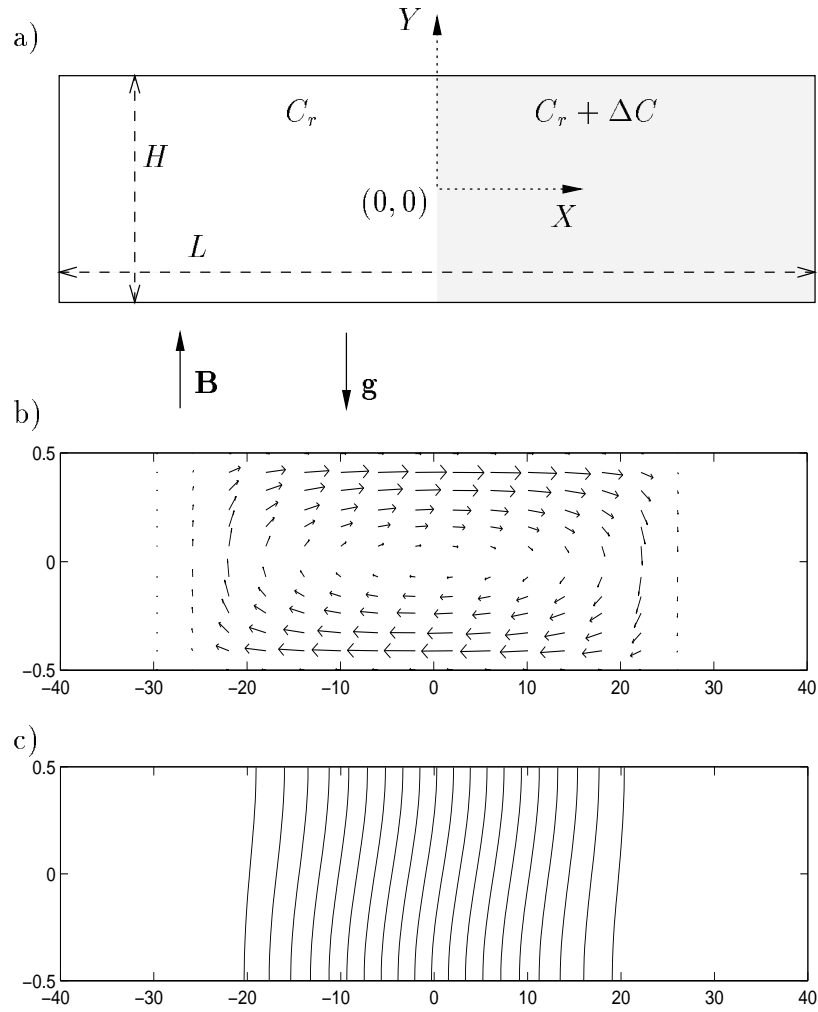


Figure 2: a) Model of the cavity with initial concentration step. b) Typical velocity field. c) Typical lines of iso-concentration. The plots in b) and c) are taken from a numerical run, the y-axis has been stretched for clarity.

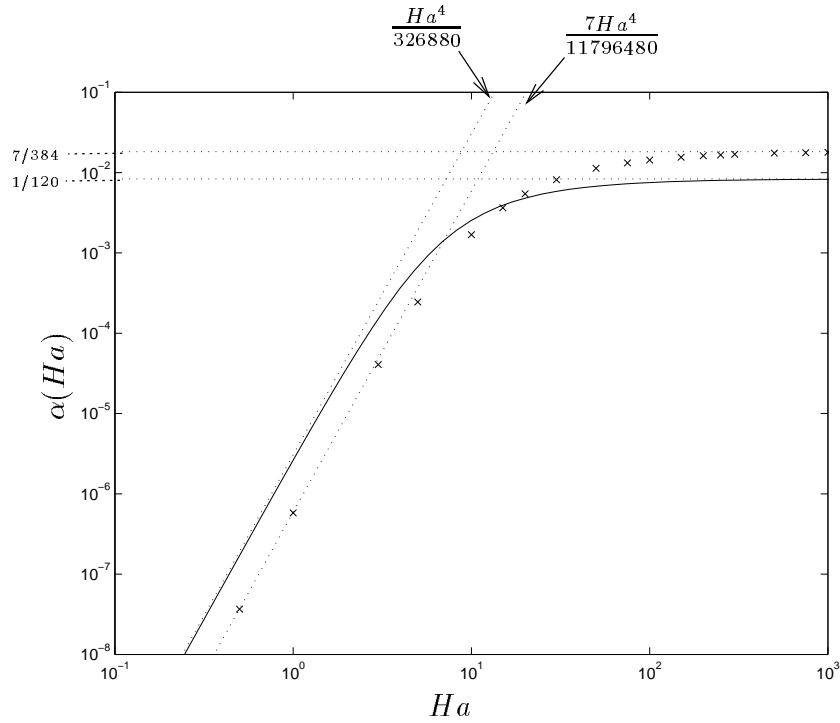


Figure 3: Asymptotic limits of the function $\alpha(Ha)$: Analytical solution for a 2D cavity from equation (12) [—]; Numerical 3D solution for a cylinder, see section 7 [$\times \times \times$]; Analytical asymptotic limits [.....].

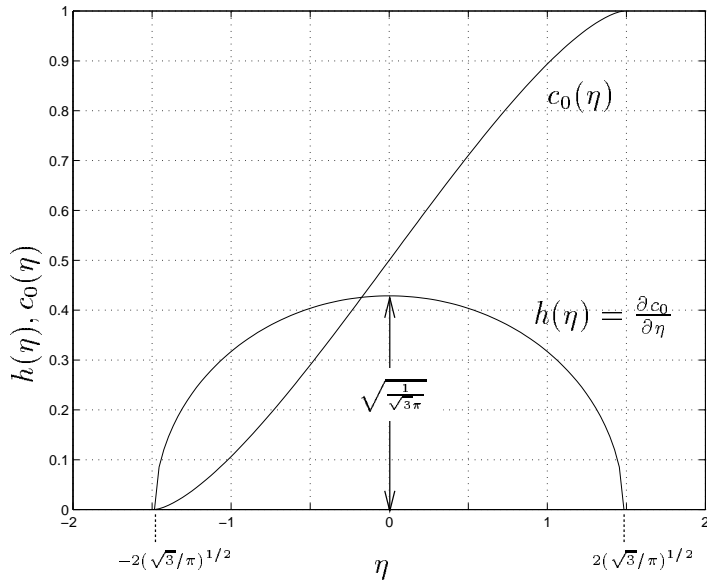


Figure 4: Concentration profile and its spatial derivative for the case of dominant convective contribution to effective diffusivity.

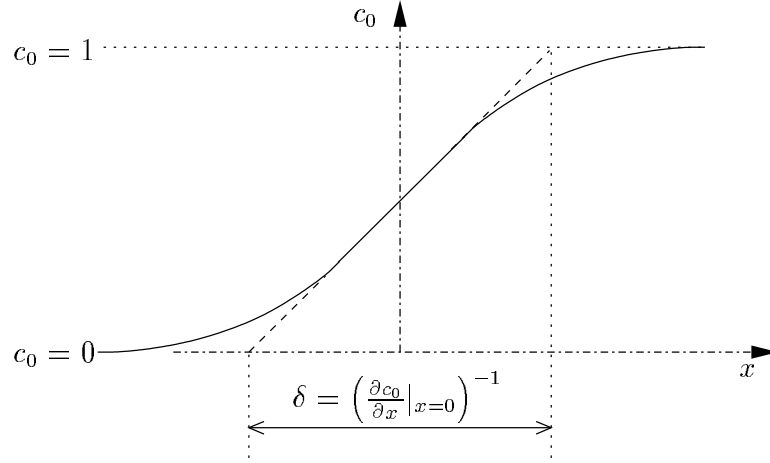


Figure 5: Diffusion length, δ , based on the averaged concentration gradient at $x = 0$.

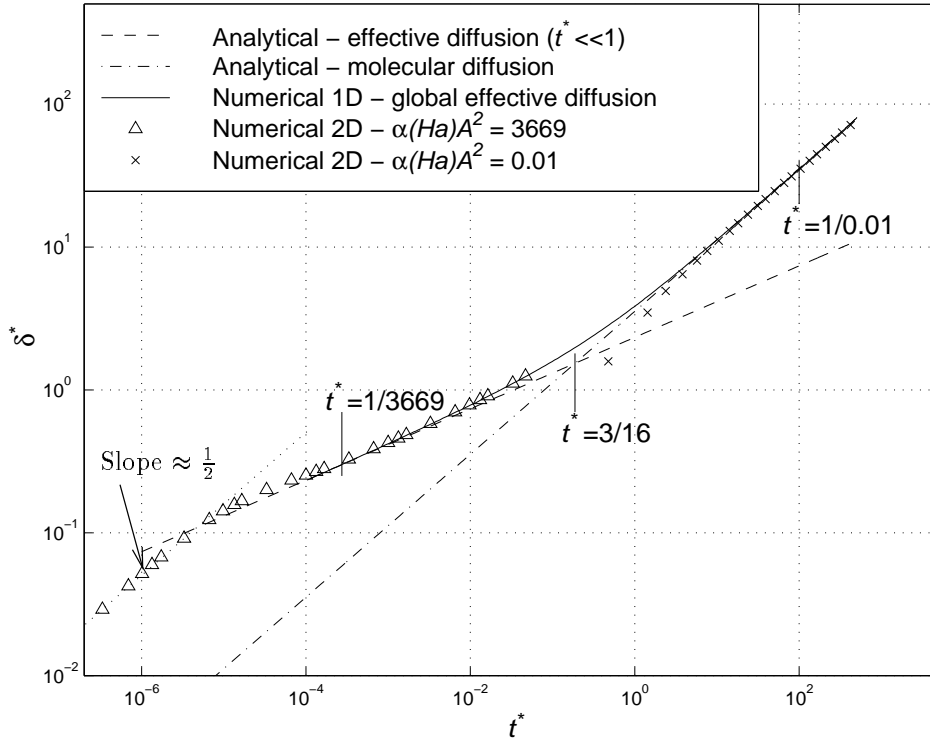


Figure 6: Diffusion length (δ^*) versus time (t^*) from asymptotic and numerical models

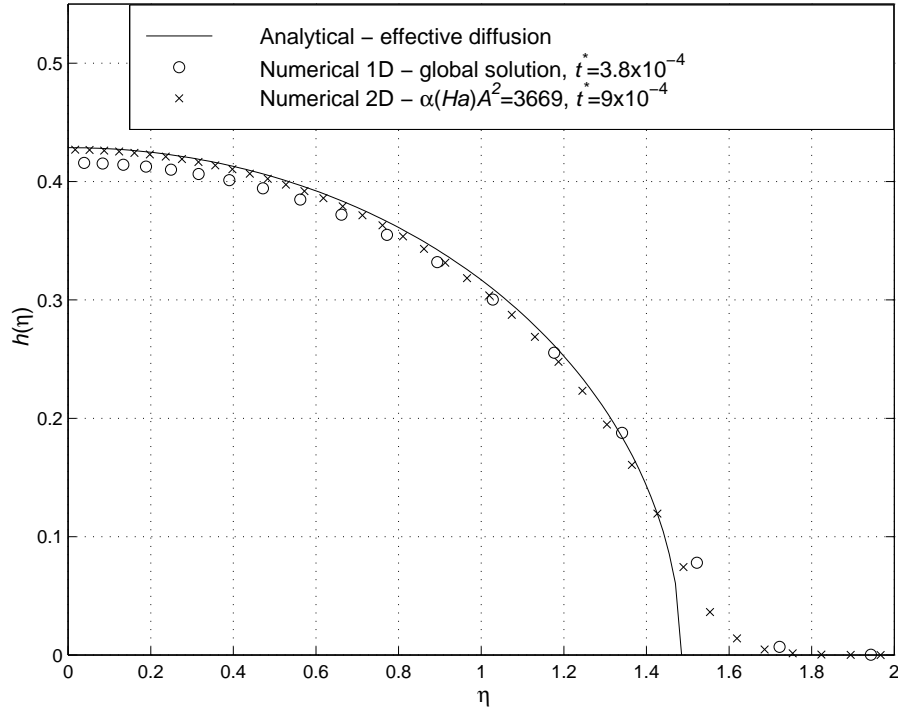


Figure 7: Time-independent profiles of averaged concentration gradient in the effective diffusivity regime: $\eta = t^{*-1/4} x^*$ versus $h(\eta) = t^{*1/4} \frac{\partial c_0}{\partial x^*}$

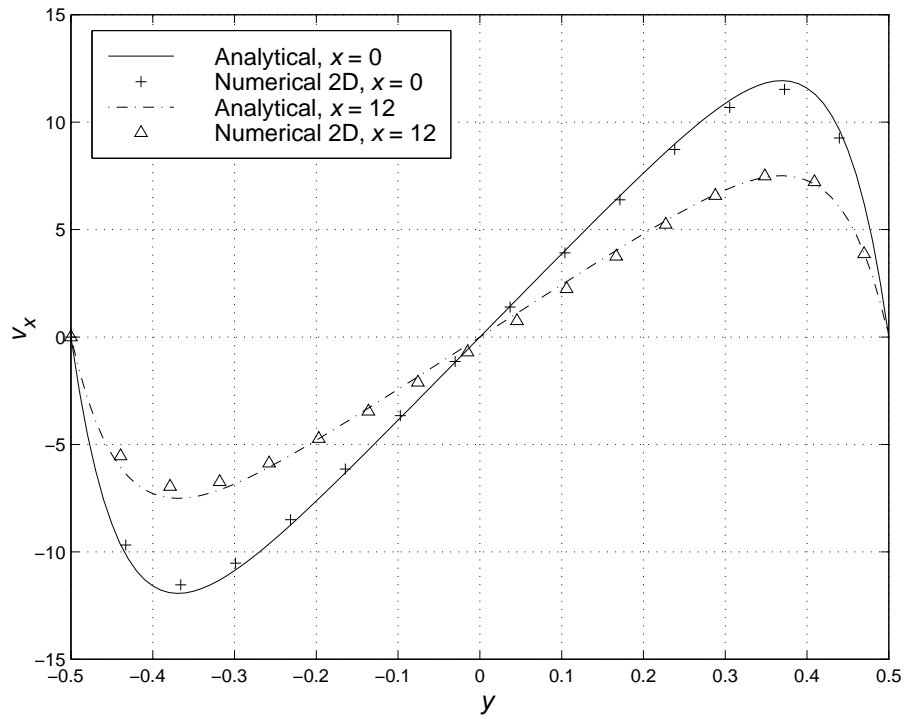


Figure 8: Analytical and numerical predictions for axial velocity profiles at $t = 3.2$ ($t^* = 8.7 \times 10^{-04}$) for $\alpha A^2 = 3669$.